J Appl Electrochem (2010) 40:933–941
DOI 10.1007/s10800-009-0030-0

ORIGINAL PAPER

Simulation of a high temperature electrolyzer

Dominique Grondin · Jonathan Deseure · Annabelle Brisse · Mohsine Zahid · Patrick Ozil

Received: 28 November 2008 / Accepted: 29 October 2009 / Published online: 21 November 2009

Abstract Based on Solid Oxide Fuel Cell (SOFC) technology, Solid Oxide Electrolysis Cell (SOEC) offers an interesting solution for mass hydrogen production. This study proposes a multiphysics model to predict the SOEC behavior, based on similar charge, mass, and heat transport phenomena as for SOFC. However, the mechanism of water steam reduction on Nickel/Yttria-Stabilized Zirconia (Ni/YSZ) cermet is not yet clearly identified. Therefore, a global approach is used for modeling. The simulated results demonstrated that a Butler–Volmer's equation including concentration overpotential provides an acceptable estimation of the experimental electric performance under some operating conditions. These simulations highlighted three thermal operating modes of SOEC and showed that temperature distribution depends on gas feeding configurations.

Keywords Hydrogen production · Solid oxide electrolysis cell · Multiphysics modeling · Diffusion phenomena · Electrochemical kinetic description

Abbreviations

A	Specific electrochemical surface area ($m^2\ m^{-3}$)
c	Concentration (mol m^{-3})
Cp	Heat capacity (J mol^{-1})
d	Mean diameter (m)
D	Diffusion coefficient ($m^2\ s^{-1}$)
F	Faraday constant (96485 C mol^{-1})
j	Electrochemical current density (A m^{-2})
J	Total current density (A m^{-2})
K	Permeability (m^2)
M	Molecular weight (kg mol^{-1})
P	Pressure (Pa)
Q	Current source (A m^{-3})
R	Universal gas constant (8.314 J $mol^{-1}\ K^{-1}$)
V	Potential (V)
T	Temperature (K)
u	Gas velocity (m s^{-1})
x	Volume fraction (−)
y	Molar fraction (−)

Greek

α	Charge transfer coefficient (−)
Γ	Reaction rate (mol $m^{-3}\ s^{-1}$)
ΔS	Water entropy formation (J $mol^{-1}\ K^{-1}$)
ε	Porosity (−)
η	Overpotential (V)
κ	Thermal conductivity (W $m^{-1}\ K^{-1}$)
Λ	Exchange current density (A m^{-2})
μ	Gas viscosity (Pa s)
ρ	Gas density (kg m^{-3})
σ	Conductivity (S m^{-1})
τ	Tortuosity (−)
Φ	Heat source (W m^{-3})

Subscripts

a	Anode
atm	Atmospheric
c	Cathode
d	Darcy
e	Electrolyte
el	Electric

D. Grondin (✉) · J. Deseure · P. Ozil
Laboratoire d'Électrochimie et de Physico-chimie des Matériaux et des Interfaces (LEPMI), UMR 5631 CNRS-INPG-UJF, 1130 rue de la piscine, ENSEEG, BP 75, 38402 Saint Martin d'Hères, France
e-mail: dominique.grondin@lepmi.inpg.fr

A. Brisse · M. Zahid
European Institute for Energy Research (EIFER), Emmy-Noether Strasse 11, 76131 Karlsruhe, Germany

eq	Equivalent
g	Grain
i,j	Binary coefficient of species *i,j*
i,k	Knudsen coefficient of species *i*
io	Ionic
i,bulk	Bulk concentration of species *i*
ox	Oxidant species
p	Pore
red	Reductive species
ref	Reference parameter
TBP	Triple phase boundary
0	Inlet condition

Superscript

eff	Effective coefficient in electrode

1 Introduction

Recently, significant research efforts are achieved to develop hydrogen economy. Hydrogen is a promising energy carrier due to its abundance, mainly in water, the high value of released energy (120 MJ kg^{-1}) and the absence of greenhouse gas emissions after combustion. Contrary to fossil fuels, hydrogen does not exist in a native state and so its use requires its production. Nowadays, the industrial mass production of hydrogen is mainly based on hydrocarbons reforming. However, water electrolysis could be the most convenient production process if it uses a clean renewable energy source. From a thermodynamical point of view, water electrolysis is more interesting at higher temperature because of a lower electricity demand. Based on the Solid Oxide Fuel Cell (SOFC) technology, a Solid Oxide Electrolysis Cell (SOEC) is a device that allows electrochemical water splitting at high temperature (700–900 °C). The cell consists on the assembly of a three-layer region involving two ceramic electrodes separated by a dense ceramic electrolyte made in the same materials as for a SOFC (Fig. 1). The hydrogen electrode is usually composed of nickel and yttrium-stabilized zirconia (YSZ) cermet. The electrolyte is made of YSZ and the oxygen electrode is based on perovskite-type oxides, which is usually strontium-doped lanthanum manganite $La_{1-x}Sr_xMnO_3$ (LSM). The electrochemical reactions in SOEC electrodes are as follows:
Cathode:

$$H_2O + 2e^- \rightarrow H_2 + O^{2-} \quad (1)$$

Anode:

$$O^{2-} \rightarrow \frac{1}{2} O_2 + 2e^- \quad (2)$$

At cathode, water steam is reduced and oxygen ions are produced (Eq. 1). Then, oxygen ions migrate through the electrolyte to the anode where oxygen molecules and electrons are released (Eq. 2). Therefore, the ionic and electronic currents produced and consumed at electrodes cross the whole SOEC and generate heat sources due to the internal cell resistance. If the cell voltage value is $\Delta H/2F$, the heat source exactly provides the heat removed by the steam electrolysis process (thermo neutral voltage). For upper and lower cell potential values, the operating modes are, respectively, endothermic and exothermic ones.

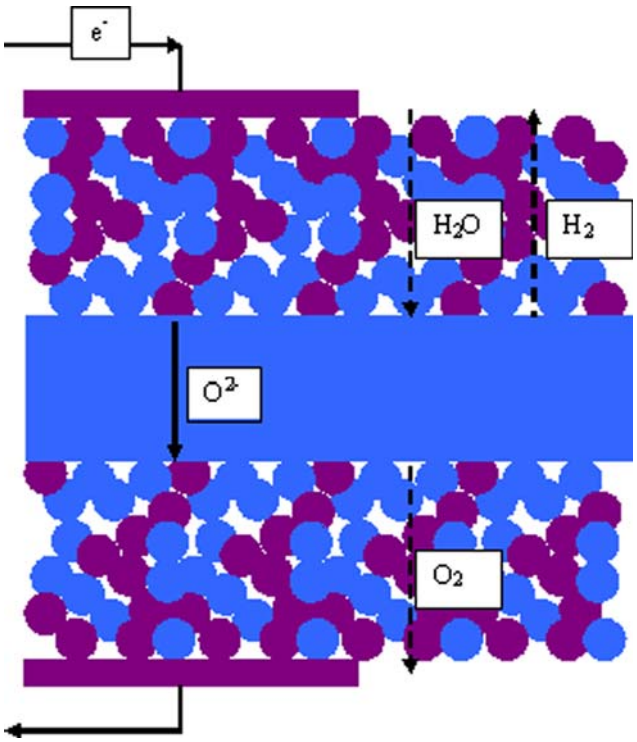

Fig. 1 Schematic view of a SOEC

The first studies devoted to SOEC were mainly experimental ones. They were carried out in the 1980s in a context of a relevant decline in oil production [1, 2]. However, these studies have been suspended until the recent development of SOFC and the investigation of reversible SOFC [3]. Many computing studies showed a great relevance for understanding and optimizing SOFC [4, 5]. Computation fluid dynamics modeling is a quite recent method to investigate the SOEC stack behavior [6]. Most of SOEC models are based on models previously developed for SOFC. Indeed, a three-dimensional SOEC model was already developed to investigate the effects of operating conditions on current densities and temperature distributions [7]. Nevertheless, few studies are available by literature regarding the water reduction kinetic on Nickel/YSZ cermet. Some experimental studies were carried out and corresponding reaction mechanisms were suggested but no further studies confirmed these proposals [3, 8].

More recently, two electrochemical models were developed for an electrolyte-supported cell and simulations were compared to experimental data [9, 10]. Both models seem to provide quite accurate predictions although there are different. Only one theoretical study was proposed for a cathode-supported SOEC, but without any comparison with experimental data [11]. The major part of available models uses a Butler–Volmer's law for activation overpotential calculation. However, this approach seems to be not precise enough since some earlier studies demonstrate that several chemical and electrochemical steps may occur.

This study proposes a multiphysics model of a single SOEC. The Butler–Volmer law pertinence is discussed for different operating conditions. The model sensitivity to electrode material properties is also studied. Finally, the effect of feeding configuration on temperature distribution is presented.

2 Model equations

The physical phenomena taking place within a SOEC have already been studied separately. SOFC and SOEC are roughly similar system. As a first step, the mathematical model developed for SOFC can be used for SOEC because of the similitude of both systems. The multiphysics approach takes into account dependence between phenomena. Assumptions are:

- gases are ideal
- constant gas velocities along gas channels
- constant electrodes ionic and thermal conductivities
- convective flow is negligible in the cathode electrode considering no increase of gas molar number and low permeability
- system is adiabatic
- ideal electrical conductivity in the current collectors

A sketch of the model structure is presented in Fig. 2. The electronic potential is solved in gray domains, the ionic potential in green domain. The water and hydrogen concentrations are solved in blue domain. The oxygen concentration is solved in brown domain. The heat balance is solved in red domain.

2.1 Charge balance

SOEC electrodes are mixed electronic–ionic conductors. The transport of each type of charge particle (e^-, O^{2-}) is described using the Ohmic's law for one elementary charge:

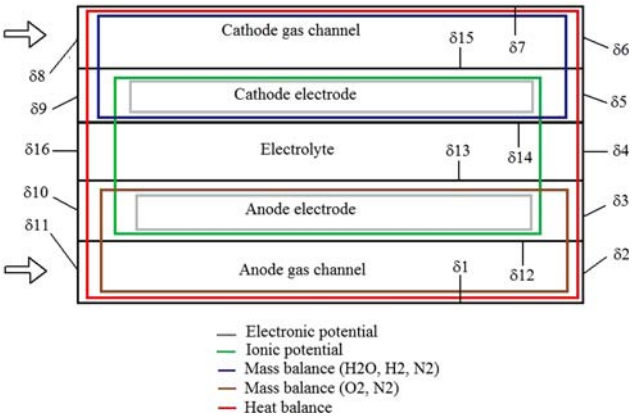

Fig. 2 Model structure sketch

$$\nabla \cdot \mathbf{J} = -\nabla \cdot \left(\sigma_{\mathrm{el,io}}^{\mathrm{eff}} \nabla V_{\mathrm{el,io}}\right) = \mathrm{Q_{el,io}} \tag{3}$$

Effective conductivity of phase i is given by the following relation where 1.6 is the tortuosity of the ionic pathway [12]:

$$\sigma_{\mathrm{i}}^{\mathrm{eff}} = \mathrm{x_i}\frac{(1-\varepsilon)}{1.6}\sigma_{\mathrm{i}} \tag{4}$$

Q is the current source term defined by relation (Eq. 5).

$$\nabla \cdot \mathbf{J} = Q_{el,io} = \pm A_{\mathbf{TPB}} j \tag{5}$$

The electrochemical reaction is assumed to take place at the triple phase boundary (TPB) i.e., the contact area between gas, electric, and ionic conductors. The specific surface area (A_{TPB}) is the surface generated by these contact areas in the electrode volume. TPBs are assumed to be uniformly distributed in the electrode volume. Since this parameter is difficult to access, one considers an A_{TPB} of 1 m^2/m^3. Yet, this specific surface area depends on microstructure. This phenomenon is taken into account by considering an exchange current density (Λ) as material properties dependent. Thus, the exchange current density is a global kinetic parameter.

In the same electrode, current source related to anion consumption/production is the opposite of that for electron (Eq. 6).

$$Q_{\mathrm{el}} = -Q_{\mathrm{io}} \tag{6}$$

In the electrolyte, no current source term is considered and a pure ionic conductivity is assumed. Electrodes electric and electrolyte ionic conductivities are considered as temperature dependent.

2.2 Mass balance

Mass transport is mainly driven by diffusion in electrodes due to concentration gradient and convection in the channels due to velocity. Both phenomena are described by the

Eq. 7. This expression differs according to the considered part of the cell.

$$\nabla \cdot (-D\nabla c) = -\mathbf{u} \cdot \nabla \mathrm{c} + \mathbf{\Gamma} \tag{7}$$

2.2.1 Hydrogen side

In the case under study, water steam is provided with hydrogen and nitrogen at cathode side. Stefan–Maxwell diffusion model is used regarding the significant difference between molecular weight of species. Moreover, Knudsen diffusion should be considered in the electrode that is a porous media. Thus, the Dusty-Gas Model (DGM) is used at cathode. Such model seems to provide the most accurate description of mass transport for SOFC anode [13]. The DGM model considers the following equivalent effective diffusion coefficient in the electrode:

$$D_{\mathrm{eq,c}}^{\mathrm{eff}} = \frac{1}{D_{\mathrm{H_2O,k}}} + \frac{1}{D_{\mathrm{H_2O,N_2}}^{\mathrm{eff}}} + (1 - y_{\mathrm{N_2}}) \times \left(\frac{1}{D_{\mathrm{H_2O,H_2}}^{\mathrm{eff}}} - \frac{1}{D_{\mathrm{H_2O,N_2}}^{\mathrm{eff}}} \right) - \frac{\beta y_{\mathrm{H_2O}}}{D_{\mathrm{H_2O,H_2}}^{\mathrm{eff}}} \tag{8}$$

with,

$$\beta = 1 - \left(\frac{M_{\mathrm{H_2O}}}{M_{\mathrm{H_2}}} \right)^{1/2} \tag{9}$$

The Knudsen diffusion coefficient of the species i ($D_{i,\ k}$) is calculated from Eq. 10 where the mean pore diameter is determined considering electrode characteristics (Eq. 11).

$$D_{i,k} = d_p \frac{\varepsilon}{3\tau} \sqrt{\frac{8RT}{\pi \mathrm{M}_i}} \tag{10}$$

$$d_p = \frac{2}{3} \frac{\varepsilon}{1-\varepsilon} d_g \tag{11}$$

The effective diffusion coefficient is the diffusion coefficient in a porous media. Different models were used to assess this coefficient [14, 15]. The models developed for SOFC or SOEC generally use the following formula [4, 16]:

$$D_{i,j}^{\mathrm{eff}} = \frac{\varepsilon}{\tau} D_{i,j} \tag{12}$$

The water consumption rate (Γ_{c}) is derived from the Faraday's law (Eq. 13).

$$\Gamma_{\mathrm{c}} = -\frac{\mathrm{Q_c}}{2F} \tag{13}$$

No Knudsen diffusion occurs within the gas channel, which is not a porous media. The equivalent diffusion coefficient is then expressed as it follows:

$$D_{\mathrm{eq,c}} = \frac{1}{D_{\mathrm{H_2O,N_2}}} + (1 - y_{\mathrm{N_2}}) \left(\frac{1}{D_{\mathrm{H_2O,H_2}}} - \frac{1}{D_{\mathrm{H_2O,N_2}}} \right) - \frac{\beta y_{\mathrm{H_2O}}}{D_{\mathrm{H_2O,H_2}}} \tag{14}$$

There is no reaction ($\Gamma = 0$) in the gas channel. All diffusion coefficients used in this model are considered as temperature dependent.

2.2.2 Oxygen side

In the oxygen electrode, oxygen molecules are produced according to the following reaction rate:

$$\Gamma_{\mathrm{a}} = \frac{Q_{\mathrm{a}}}{4F} \tag{15}$$

The oxygen flux in the electrode and at the boundary results in multiphysics computation. Since the electrolyte is a dense material, all the oxygen produced in the electrode volume will flow out in the gas channel. Total pressure in this electrode increases and consequently a permeation flux has to be computed. Gas velocity in the anode electrode (u_{a}) is given by the Darcy's law (Eq. 16). Gas viscosity (μ) is here dependent on both composition and temperature [17, 18]. Electrode permeability (K) is determined by the Kozeny–Carman relation (Eq. 17) [19] and the oxygen effective diffusion coefficient is calculated according to the Bosanquet formula (Eq. 18) [9].

$$u_{\mathrm{a}} = -\frac{K}{\mu_{\mathrm{O_2,\ N_2}}} \nabla p \tag{16}$$

$$K = \frac{\varepsilon^3}{72\tau(1-\varepsilon)^2} d_g^2 \tag{17}$$

$$D^{\mathrm{eff}} = \left(\frac{1}{D_{\mathrm{O_2,N_2}}^{\mathrm{eff}}} + \frac{1}{D_{\mathrm{O_2,k}}} \right)^{-1} \tag{18}$$

In the gas channel, no reaction occurs ($\Gamma = 0$). A Fick's diffusion model is used since difference between molecular weight of species is not really significant. The diffusion coefficient considered in the gas channel is $D_{\mathrm{O_2,N_2}}$.

2.3 Heat balance

Temperature is a key parameter in such system due to the dependence of many parameters on it. Moreover, materials are really sensitive to temperature gradient. While SOEC operates at high temperature, 800 °C in the present case, radiative heat transfer becomes non-negligible. However, a previous study demonstrated that radiative heat transfer inside the cell could be neglected ahead of conductive transfer for a SOFC [20]. Then, only convection and conduction phenomena are taken into account to describe heat transfer in the cell under study. Heat balance can be expressed as:

$$\nabla.(-\kappa\nabla T) = \Phi - \rho C\mathbf{p}\mathbf{u}\cdot\nabla T \quad (19)$$

Gas physical properties depend on both composition and temperature [17, 18]. The heat source (Φ) varies according to the considered part of the cell. Electrochemical reaction irreversibilities (ηQ) are considered in addition to the Joule's effect in the electrodes ($\mathbf{J}\cdot\nabla V$) (Eqs. 20, 21). An ionic Joule's effect only occurs in the electrolyte (Eq. 22) and there is no heat source in the gas channels. Overpotentials involved in a solid oxide electrolysis cell will result in heat generation due to entropy generation. The heat source mainly results from entropy change of the electrochemical and the water splitting reactions [21]. We assume that the entropy change of the water splitting reaction is most significant at the cathode side since water molecule is split and hydrogen is formed at this electrode.

$$\Phi_c = \left(\frac{-T\Delta S}{2F} + \eta\right)Q_c - \mathbf{J}\cdot\nabla V_{el} - \mathbf{J}\cdot\nabla V_{io} \quad (20)$$

$$\Phi_a = \eta Q_a - \mathbf{J}\cdot\nabla V_{el} - \mathbf{J}\cdot\nabla V_{io} \quad (21)$$

$$\Phi_e = \mathbf{J}\cdot\nabla V_{io} \quad (22)$$

2.4 Charge transfer model

The electrochemical current density (j) is a relevant variable since it acts in all balances and it is linked to electrochemical reaction kinetic data. There is a poor literature about water steam reduction kinetic on Nickel/YSZ cermet and oxygen ion oxidation on LSM. It is thus difficult to have an accurate expression for j. However, different models exist for current density calculation from overpotential. In this study, Butler–Volmer's with concentration overpotential (Eq. 23) is used to simulate the electric cell performance [10].

$$j_{a,c} = \Lambda_{a,c}\left(\frac{c_{red}}{c_{red,bulk}}\exp\left(\frac{2\alpha F\eta}{RT}\right) - \frac{c_{ox}}{c_{ox,bulk}}\exp\left(\frac{-2(1-\alpha)F\eta}{RT}\right)\right) \quad (23)$$

$$\eta = V_{el} - V_{io} \quad (24)$$

where $c_{i,\ bulk}$ is the concentration at the gas inlet.

3 Numerical model

The mathematical model previously defined is solved using the code of COMSOL Multiphysics®. Geometry and boundary conditions have to be defined before solving the set of partial differential equations and performing simulations with the software.

3.1 Geometry and mesh

This study aims to investigate the behavior of a single circular SOEC. Some experimental data are used in this study to check model accuracy. These data are obtained from a single circular SOEC where it is assumed that gas diffusion media allow a good uniformity of gas velocity and current collectors ensure the equipotential. These assumptions were checked by 3D modeling of the accurate geometry [22]. The geometry will thus include only electrodes, electrolyte, and gas channels. Only a cross section of the cell along the radius is modeled due to symmetry (Fig. 3). The cell dimensions and characteristics are gathered in Table 1. The cell operates at atmospheric pressure. Inlet gas temperature is 800 °C.

A mapped mesh is used to obtain a reasonable number of degrees of freedom allowing calculation convergence within an acceptable computation time. The number of degrees of freedom is here 26 733 and the minimum element quality is 0.0359.

3.2 Boundary conditions

This section presents the boundary conditions used to solve each balance. Boundaries can be located in Fig. 2.

The present multiphysics problem uses six equations needing boundary conditions for solving: electric charge balance (Table 2), ionic charge balance (Table 3), Darcy's law (Table 4), water mass balance (Table 5), oxygen mass balance (Table 6), and heat balance (Table 7).

The voltage, as the difference between the potentials at the anode and cathode, is a parameter for the simulation to calculate the polarization curves. The linear system solver is here *Direct PARDISO*. Main parameter values used for the resolution are gathered in Table 8.

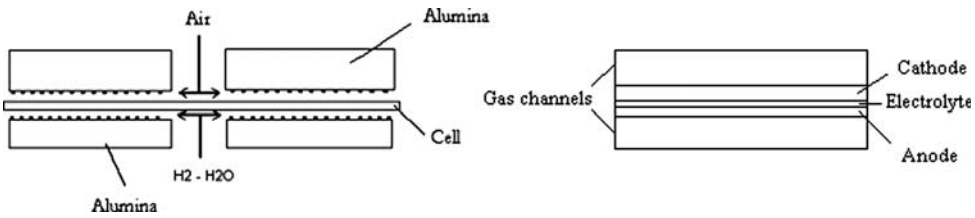

Fig. 3 Schematic view of the experimental cell (**a**) and the geometry for modeling (**b**)

Table 1 Cell characteristics

Cathode thickness [m]	240×10^{-6}
Electrolyte thickness [m]	7×10^{-6}
Anode thickness [m]	20×10^{-6}
Cell radius [m]	39×10^{-3}
Gas channels height [m]	1×10^{-3}
Electrodes porosity (ε) [−]	0.3
Anode tortuosity (τ_a) [−]	1.7
Cathode tortuosity (τ_c) [−]	6
Electrodes mean grain diameter (d_g) [m]	10×10^{-6}
Nickel electronic conductivity (σ_{Ni}) [S/m]	4.5×10^5
LSM electronic conductivity (σ_{LSM}) [S/m]	1.6×10^5
YSZ ionic conductivity (σ_{YSZ}) [S/m]	5
Nickel volume fraction (x_{Ni}) [−]	0.4
LSM volume fraction (x_{LSM}) [−]	0.5
Cathode thermal conductivity (κ_c) [W/m/K]	11
Electrolyte thermal conductivity (κ_e) [W/m/K]	2.7
Anode thermal conductivity (κ_a) [W/m/K]	6

Table 2 Electric charge balance boundary conditions

Setting	$\delta\Omega$ 12	$\delta\Omega$ 15	$\delta\Omega$ 3, 5, 9, 10, 13, 14
Type	Electric potential	Electric potential	Electric insulation
Expression	V_a	V_c	$\mathbf{n} \cdot \mathbf{J} = 0$

Table 3 Ionic charge balance boundary conditions

Setting	$\delta\Omega$ 3, 4, 5, 9, 10, 12, 13, 14, 15, 16	$\delta\Omega$ 13, 14
Type	Electric insulation	Continuity
Expression	$\mathbf{n} \cdot \mathbf{J} = 0$	$\mathbf{n} \cdot (\mathbf{J}_1 - \mathbf{J}_2) = 0$

Table 4 Darcy's law boundary conditions

Setting	$\delta\Omega$ 3, 10	$\delta\Omega$ 12	$\delta\Omega$ 13
Type	Insulation	Pressure	Outflow
Expression	$-\frac{K}{\eta}\nabla p \cdot \mathbf{n} = 0$	p_{atm}	$\frac{JM_{O_2}}{4F\rho}$

Table 5 Water mass balance boundary conditions

Setting	$\delta\Omega$ 8	$\delta\Omega$ 5, 7, 9, 14	$\delta\Omega$ 6
Type	Concentration	Insulation	Convective flux
Expression	$y_{H_2O,0}\frac{p_{atm}}{RT_o}$	$\mathbf{n} \cdot (-D\nabla c + c\mathbf{u}) = 0$	$\mathbf{n} \cdot (-D\nabla c) = 0$

Table 6 Oxygen mass balance boundary conditions

Setting	$\delta\Omega$ 11	$\delta\Omega$ 1, 3, 10, 13	$\delta\Omega$ 2
Type	Concentration	Insulation	Convective flux
Expression	$y_{O_2,0}\frac{p_{atm}}{RT_o}$	$\mathbf{n} \cdot (-D\nabla c + c\mathbf{u}) = 0$	$\mathbf{n} \cdot (-D\nabla c) = 0$

4 Model parameters estimation

4.1 Charge transfer model accuracy

Simulations are performed with the expression of the Faradic current density given by the Eq. 23. A comparison with experimental polarization curves (cell potential vs. current density) obtained under steady-state conditions at 800 °C is carried out to check the charge transfer model. The exchange current density is tuned to fit the experimental polarization curves. Figure 4 presents the best fit obtained for $\Lambda_a = 2.12 \times 10^8$ A/m^2 and $\Lambda_c = 6.4 \times 10^6$ A/m^2. The Butler–Volmer's law including concentration overpotential provides a good prediction of the electric cell performance under this operating conditions (inlet water molar fraction = 70%). This model may be considered as calibrated.

4.2 Influence of effective diffusion coefficient assessment

Before using the calibrated model to predict cell behavior in various operating conditions, it is necessary to check its predictive ability for another inlet water molar fraction (30%). The model appears unable to predict the electric cell behavior as shown in Fig. 5. Diffusion phenomenon seems to be critical at this concentration. As said previously, several laws are available for effective diffusion coefficient calculation. Bruggeman's law (Eq. 25) is used to observe effective diffusion coefficient influence on simulation results [23].

$$D_{ij}^{\text{eff}} = D_{ij}\varepsilon^{\tau} \tag{25}$$

Tortuosity (τ) is an estimated parameter that is impossible to be properly determined with the cell under study. In some previous study, the tortuosity was considered as a tuning parameter to fit experimental data [4]. Literature provides values varying between 3.5 [4] and 10 [16] for SOFC studies. Here, the Bruggeman's law with a tortuosity set to 4.8 seems to be the most suitable law to describe diffusion phenomena in the cell (Fig. 5). A good agreement is then also observed with an inlet water molar fraction of 70% as shown in Fig. 6.

Porosity and mean grain diameter are estimated parameters. Figure 7 shows the influence of these parameters on simulated polarization curves. Exchange current density (Λ) depends on electrode microstructure. This influence is considered using the following expression [12]. Reference parameters are those used in the calibrated model.

$$\Lambda = \Lambda_{\text{ref}}\left(1 - \frac{\varepsilon - 0.26}{0.74}\right)\frac{d_{g,\text{ref}}^3}{d_g^3} \tag{26}$$

Table 7 Heat balance boundary conditions

Setting	$\delta\Omega$ 8, 11	$\delta\Omega$ 1, 3, 4, 5, 9, 10, 16	$\delta\Omega$ 2, 6	$\delta\Omega$ 12, 13, 14
Type	Temperature	Thermal insulation	Convective flux	Continuity
Expression	T_o	$\mathbf{n}\cdot(-\kappa\nabla T+\rho CpuT)=0$	$\mathbf{n}\cdot(-\kappa\nabla T)=0$	$-\mathbf{n}_1\cdot(-\kappa\nabla T_1)-\mathbf{n}_2\cdot(-\kappa\nabla T_2)=0$

Table 8 Input data

Pressure (P_{atm}) [Pa]	1.013×10^5
Temperature (T_0) [°C]	800
Gas velocities (u) [m/s]	1.25
Inlet water steam molar fraction ($y_{H_2O,0}$) [−]	0.7
Inlet oxygen molar fraction ($y_{O_2,0}$)	0.21
Charge transfer coefficient (α) [−]	0.5

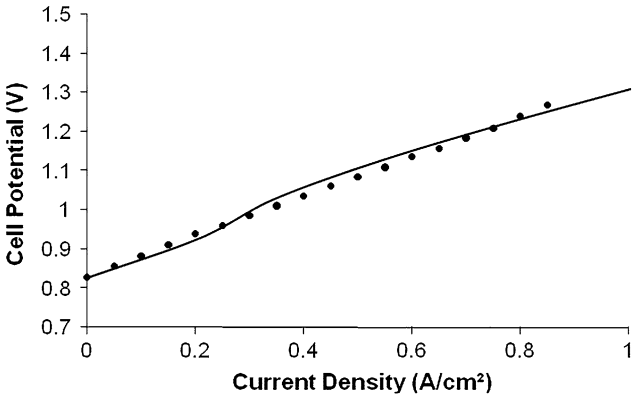

Fig. 4 Comparison between simulated polarization curves using Butler–Volmer's law with concentration overpotential (—) and the experimental one (●) for 70% inlet water molar fraction

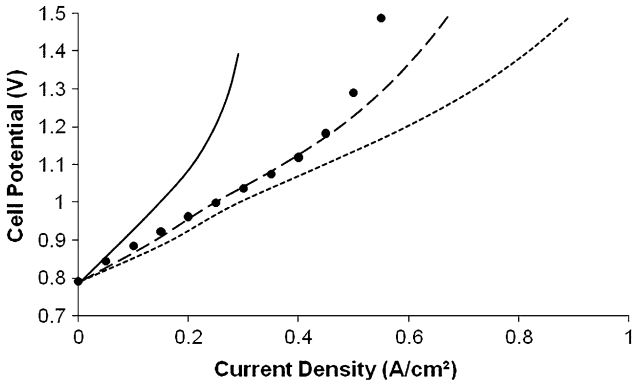

Fig. 5 Comparison between simulated polarization curves using the Bruggeman's law with $\tau = 6$ (—), $\tau = 4.8$ (– –), the calibrated model (- - -) and the experimental polarization curve (●) for 30% inlet water molar fraction

Several values are used for porosity and mean grain diameter and in any case, a very good agreement between simulated and experimental curves is obtained. Observed discrepancy may not be due to only diffusion phenomena

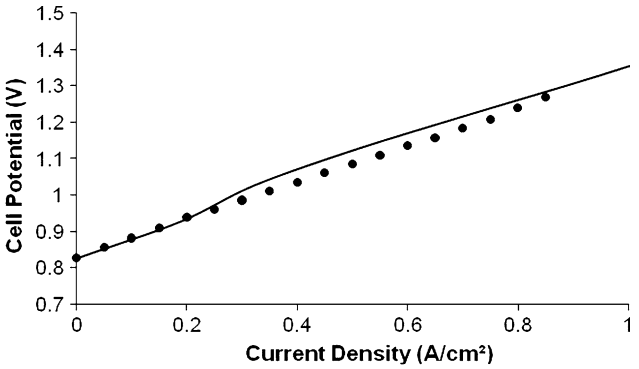

Fig. 6 Comparison between simulated polarization curves using the Bruggeman's law ($\tau = 4.8$) (—) and the experimental one (●) for 70% inlet water molar fraction

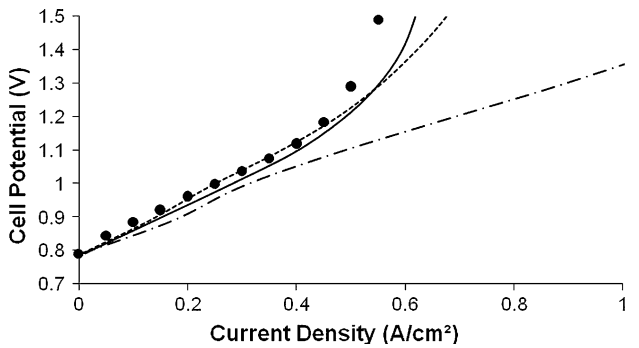

Fig. 7 Comparison between simulated polarization curves with $\varepsilon = 0.3$ and $d_g = 10$ μm (- - -), $\varepsilon = 0.4$ and $d_g = 10$ μm (– · –), $\varepsilon = 0.3$ and $d_g = 6.8$ μm (—) and the experimental one (●) for 30% inlet water molar fraction

and microstructure descriptions (Fig. 7). Indeed, the Butler–Volmer's law assumes a single step electrochemical water reduction. Such assumption may be inadequate for low water steam partial pressure according Schouler et al. [8]. For 30% inlet water molar fraction, the Butler–Volmer's law cannot predict the cell electrical behavior.

5 Results

5.1 Overpotential distribution

One considers the calibrated model at 70% water molar fraction with the Bruggeman's law for effective diffusion coefficient assessment. Our simulation results exhibit

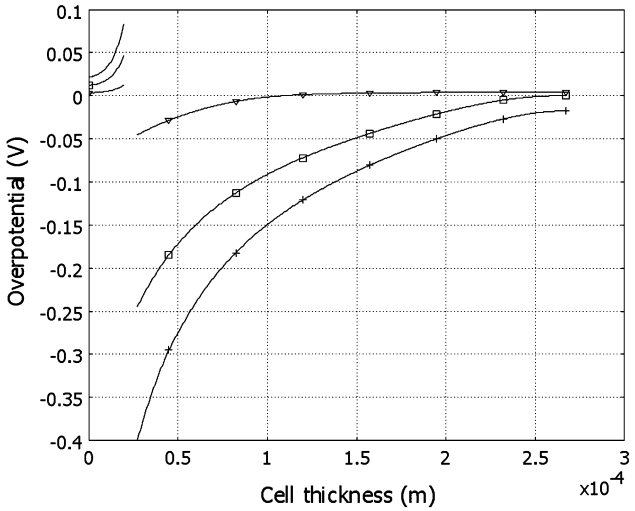

Fig. 8 Overpotential distribution in a cross section of the cell for 0.1 (▼), 0.5 (□) and 1 (+) A/cm^2

negative overpotential at the cathode and positive at the anode (Fig. 8). Moreover, the absolute highest overpotential value in both electrodes is located at the electrode/electrolyte interface. Higher overpotentials are obtained at the cathode side due to diffusion process at this electrode.

The concentration overpotential seems to be a critical phenomenon at the cathode side. Our simulations show the concentration gradient along the gas channel and within the cathode (Fig. 9). Decreasing water concentration for increasing current density has been demonstrated by our simulations.

5.2 Temperature distribution

A change in feeding configuration is investigated using the calibrated model for 70% inlet water molar fraction. Only oxygen flow direction has been changed to compute the

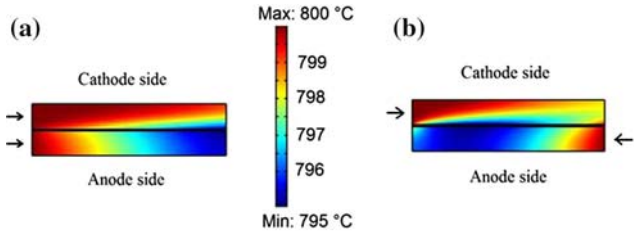

Fig. 10 Temperature profile in a co- (**a**) and a counter-flow (**b**) configuration for a cell potential of 1.1 V

counter-flow configuration. Concentration profiles and polarization curve appear to be similar in both configurations (not presented in this article). The most interesting results concern temperature profile. As shown in Fig. 10, temperature distributions are different according to feeding configuration. Cell border temperatures have the same magnitude in a counter-flow configuration contrary to co-flow configuration. Another remarkable result is that three thermal behaviors are observed depending on the cell potential value. For a cell voltage lower than 1.3 V, a cooling effect is noted. Around 1.3 V, the cell and gas temperature are quite constant while it increases for higher potentials. This phenomenon is due to the endothermic water splitting reaction. At a critical value of cell potential (thermo neutral voltage), the Joule's effect heat source compensates the reaction heat consumption. Temperature is then constant (thermo neutral mode). Figure 11 shows temperature profiles in an exothermal mode i.e., for cell potential higher than 1.3 V in both configurations.

6 Conclusions

A multiphysics model of a solid oxide electrolysis cell has been developed and solved using COMSOL

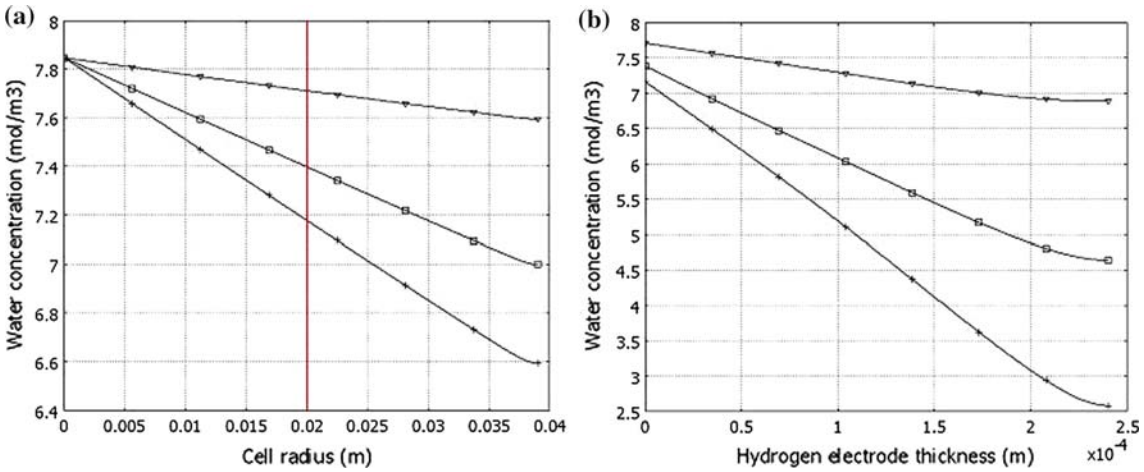

Fig. 9 Water concentration distribution along the cell radius in the gas channel (**a**) and in the hydrogen electrode in the middle of the cell (**b**) for 0.1 (▼), 0.5 (□) and 1 (+) A/cm^2

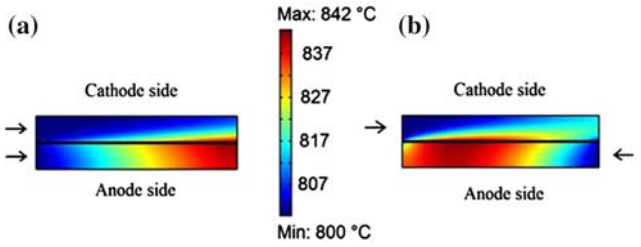

Fig. 11 Temperature profile in a co- (**a**) and a counter-flow (**b**) configuration for a cell potential of 1.6 V

Multiphysics® 3.4 software. The model using Butler–Volmer's law with concentration overpotential allows a good electric prediction for high inlet water partial pressure. However, a particular attention must be paid to the electrode materials' properties estimation since the model is highly sensitive to them. Simulation data provide detailed local profiles of potential, gas composition, and temperature. However, a more accurate electrochemical model for water reduction should be investigated to describe the high current density operation at low inlet water concentration. In addition, this study emphasizes the thermal behavior of the SOEC. Therefore, the three thermal modes of SOEC have been observed in accordance with theory. Simulations showed that temperature distribution also depends on feeding configurations. Thanks to the simulations, we can predict operating conditions for the lower risk for the cell life.

References

1. Dönitz W, Streicher R (1980) Chem Ing Tech 52:436
2. Dönitz W, Erdle E (1985) Int J Hydrogen Energy 10:291
3. Eguchi K, Hatagishi T, Arai H (1996) Solid State Ion 86–88:1245
4. Shi Y, Cai N, Li C (2007) J Power Sour 164:639
5. Ji Y, Yuan K, Chung JN, Chen YC (2006) J Power Sour 161:380
6. Ni M, Leung MKH, Leung DYC (2006) Chem Eng Technol 30:587
7. Herring JS, O'Brien JE, Stoots CM et al (2007) Int J Hydrogen Energy 32:440
8. Schouler EJL, Kleitz M, Forest E et al (1981) Solid State Ion 5:559
9. Ni M, Leung MKH, Leung DYC (2006) Chem Eng Technol 29:636
10. Ni M, Leung MKH, Leung DYC (2007) Electrochim Acta 52:6707
11. Udagawa J, Aguiar P, Brandon NP (2007) J Power Sour 166:127
12. Deseure J, Bultel Y, Dessemond L et al (2005) Electrochim Acta 50:2037
13. Suwanwarangkul R, Croiset E, Fowler MW et al (2003) J Power Sour 122:9
14. Ho FG, Strieder W (1980) J Chem Phys 73:6296
15. Mu D, Liu ZS, Huang C et al (2007) J Porous Mater 14:49
16. Andreassi L, Rubeo G, Ubertini S et al (2007) Int J Hydrogen Energy 32:4559
17. Reid RC, Sherwood TK (1958) The properties of gases and liquids. McGraw-Hill, New York
18. Perry RH, Chilton CH, Green DW (eds) (1997) Perry's chemical engineer's handbook, 7th edn. McGraw-Hill, New York
19. Jeon DH, Nam JH, Kim CJ (2006) J Electrochem Soc 153:A406
20. Damm DL, Fedorov AG (2005) J Power Sour 143:158
21. Ni M, Leung MKH, Leung DYC (2007) Int J Hydrogen Energy 32:4648
22. Grondin D, Deseure J, Zahid M et al (2008) Comput Aided Chem Eng 25:841
23. Hwang JJ, Chen PY (2006) Int J Heat Mass Transf 49:2315